FULL SPHERE FAR-FIELD ANTENNA PATTERNS OBTAINED USING A SMALL PLANAR SCANNER AND A POLY-PLANAR MEASUREMENT TECHNIQUE

Stuart F. Gregson
Nearfield Systems Inc.
19730 Magellan Drive, Torrance, CA 90502-1104, USA

Clive G. Parini
Queen Mary University of London
Mile End Road, London E1 4NS, UK

John McCormick
SELEX SAS
Crewe Road North, Crewe Toll, Edinburgh, EH5 2XS, UK

ABSTRACT

This paper presents an overview of work carried out in developing the probe-corrected, poly-planar near-field antenna measurement technique [1, 2, 3, 4, 5]. The poly-planar method essentially entails a very general technique for deriving asymptotic far-field antenna patterns from near-field measurements taken over faceted surfaces.

The probe-corrected, poly-planar near-field to far-field transformation, consisting of an innovative hybrid physical optics (PO) [6] plane wave spectrum (PWS) [7] formulation, is summarised, and the importance of correctly reconstructing the normal electric field component for each of the discrete partial scans to the success of this process is highlighted. As an illustration, in this paper the poly-planar technique is deployed to provide coverage over the entire far-field sphere by utilising a small planar facility to acquire two orthogonal tangential near electric field components over the surface of a conceptual cube centred about the antenna under test (AUT). The success of the poly-planar technique is demonstrated through numerical simulation and experimental measurement. A discussion into the limitations of the partial scan technique is also presented.

Keywords: Poly-Planar, Physical Optics, Near-field, Antenna Measurement, Probe Pattern Correction.

1.0 Introduction

Hitherto, the problem of truncation in near-field data acquired over a planar surface has been partially addressed by combining data sets that have been acquired via a series of coplanar transforms, *e.g.* translations or rotations. The primary truncation error determines the polar angle off boresight out to which any far-field pattern can be predicted from near-field measurements, whilst the secondary truncation error limits the extent to which the pattern within this angle can be accurately predicted. Partial scans that can be combined to produce the composite data set and will require that the position of the AUT, relative to the scan plane, be spatially transformed between scans so that the combined data set represents a larger scan area than that actually available via a single scan can be effectively used to extend this angle of validity.

Techniques for rigorously applying vector isometric rotations (*i.e.* transformations without change of shape or size), to antenna patterns, usually used to correct measurements taken when the AUT is not correctly aligned to the range, readily offer the possibility of producing antenna measurements, based upon partial scan techniques, that are *not* coplanar. By rotating the AUT about one or *more* spatial axes, which are not necessarily normal to the scan plane, and combining the resulting partial scans it is clearly possible to increase the angle of validity and level of accuracy of a planar measurement.

The poly-planar technique is a novel measurement and transformation process that can be employed to extend the capability of existing planar facilities so that they can successfully characterise either larger antennas, or lower gain antennas, than would otherwise have been the case at the expense of only a comparatively small increase in the amount of computational effort required. Furthermore, as this is essentially a partial scan technique, it does not require that the AUT be moved during the acquisition of the individual partial scans, instead allowing the antenna assembly to be carefully repositioned in "slow time". Thus, it can be seen to be of utility in the characterisation of either gravitationally sensitive antennas or, in the measurement of active electronically scanned array (AESA) antennas which require considerable amounts of supporting infrastructure with the requirement for, large

connecting umbilicals which are used to supply power, cooling, control, *etc.* to the AUT.

2.0 Difficulties with Conventional Auxiliary Rotation Partial Scan Approaches

Previously biscan (consisting of two intersecting partial scans), triscan (consisting of three intersecting partial scans), *etc.* measurements utilising conventional plane wave spectrum based transformations have yielded some success. However, in computer simulations, these transformations have always been found to introduce some error that manifests itself in the form of a high frequency ripple on the far field pattern and is most noticeable at very wide angles. Within the most general integral transform derivation of the PWS representation of electromagnetic fields, the partial derivatives of the boundary conditions with respect to each of the axes are obtained by means of two operator substitutions. These operator substitutions are assumed to hold everywhere and are used to reduce the scalar Helmholtz equation, which is a second order partial differential equation, to an ordinary differential equation [5]. When viewed in this way, the Fourier transform is used as a way of separating the variables.

Unfortunately, if the boundary conditions are only piecewise smooth, the integration by parts that is performed within the derivation of these operator substitutions becomes impossible [4]. The implication of this is that the function must be considered as a distribution, *i.e.* a generalised function and crucially, any derivatives must also be considered as generalised derivatives. Thus, provided the fields are sampled at, or preferable higher than, the Nyquist rate over the sampling surface, and provided the surface of integration is smooth, *i.e.* the function describing the surface profile, and all of the first partial derivatives are continuous, reliable far-field data can be obtained. However, as soon as the surface profile is not smooth, as is the case for the poly-planar technique, a spurious high frequency ripple can be observed. The amplitude of this ripple is dependent upon the magnitude of the ordinary discontinuity and the intensity of the field in that region. Thus, the problem becomes, how to calculate the probe-corrected electromagnetic six-vector over the partial scans whereupon other, less restricted, transformation techniques can be utilised.

3.0 Reconstruction of Normal Field Component

Conventionally the normal field components are not measured; instead they are recovered from the tangential components via an application of the plane wave condition $\underline{k} \cdot \underline{E} = 0$. If however, the sampled data set is truncated, the reconstructed normal field component will be in error. This is obviously a problem as partial scans are by definition truncated. Furthermore, this field component is required before the partial data sets can be combined, as the principal of superposition requires that each component be resolved onto the *same* polarisation basis. These difficulties can be resolved if the normal field component is sought over the surface of each partial plane. All three orthogonal field components can then be transformed to the far-field whereupon the partial data sets can be combined in the usual way. Using a near-field simulator, the normal field component was obtained from the tangential components and results from this comparison can be found in Figure 1 below.

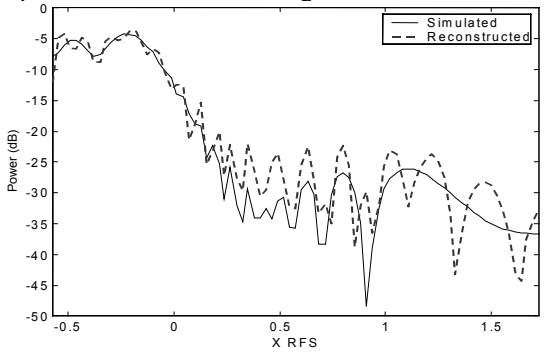

Figure 1 Plot of simulated and reconstructed normal field component without windowing

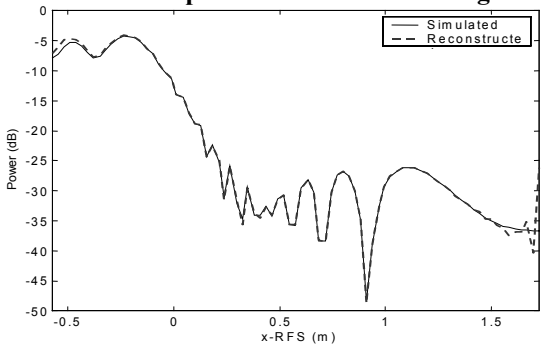

Figure 2 Plot of simulated and reconstructed normal field component with windowing

The spurious high frequency ripple that is present in the reconstructed normal field component can be removed by windowing the tangential field components before transforming to the angular spectrum. Importantly, as the magnetic field is often calculated from the electric field and the direction of propagation, these fields could potentially contain the same error. The "convoluted" normal spectral component can be obtained directly from the plane wave condition whereupon it can be inversely transformed to obtain the "windowed" normal field component. The windowing function can then be divided out to obtain reliable results such as those presented in Figure 2. The divergence between reconstructed and

exact results is a result of the compensation for the windowing function and in practice is displaced out of the region of interest by simply over-scanning the near-field data by a few samples. The derivation of the expressions that are used to correct the measured near-field data for the directive properties of the measuring probe relied upon the validity of the plane wave condition. Thus, the normal field component utilised implicitly within these expressions will be recovered erroneously for the case where the near-field data set is truncated. Thus, truncated measurements that are corrected with these expressions will also be in error. Again, such difficulties can be avoided with the application of a suitable windowing function. A proof of the validity of the use of windowing functions can be found presented in [4, 5]. The normal field component, here designated E_z can be obtained from the tangential field components, E_x E_y, through the use of the plane wave condition to obtain,

$$E_z(x,y) = \frac{1}{w(x,y)} \Im^{-1}\left\{ -\frac{\alpha}{\gamma} \Im\{w(x,y)E_x(x,y)\} - \frac{\beta}{\gamma} \Im\{w(x,y)E_y(x,y)\} \right\} \quad (1)$$

Where $\Im$ represents the 2D Fourier transform of the near-field on a plane and $\Im^{-1}$ its inverse, w is the spatial windowing function, α, β and γ are the direction cosines in the x-, y- and z-axes respectively so that $\underline{\hat{u}} = \alpha \underline{\hat{e}_x} + \beta \underline{\hat{e}_y} + \gamma \underline{\hat{e}_z}$ where $\underline{\hat{u}}$ is a unit vector which is simply related to the direction of propagation $\underline{k} = k_x \underline{\hat{e}_x} + k_y \underline{\hat{e}_y} + k_z \underline{\hat{e}_z} = k_0 \left(\alpha \underline{\hat{e}_x} + \beta \underline{\hat{e}_y} + \gamma \underline{\hat{e}_z} \right)$. This equality holds for any of the normal windowing functions that are absolutely integrable and are non-zero.

The derivation of the expressions that are used to correct the measured near-field data for the directive properties of the measuring probe also rely upon the validity of the plane wave condition. The normal field component will be erroneously recovered for the case where the near-field data set is truncated. Thus, truncated measurements that are corrected with these expressions will also be in error. Again, such difficulties can be avoided with the application of a suitable windowing function. So, taking the approach of Brown [6] and extending to the general dual probe case and using a similar approach to that described above, a more important proof demonstrating the validity of the use of windowing functions when applying probe pattern correction can be obtained [4]. Thus, the corrected x- and y-polarised tangential electric field component can be obtained from,

$$a_x = \frac{1}{w} \Im^{-1}\left\{ \frac{1}{\gamma D} \left[\left(1-\alpha^2\right) \left(C_x \Im\{ws_x\} + B_y \Im\{ws_y\} \right) + \alpha\beta \left(C_y \Im\{ws_x\} - B_x \Im\{ws_y\} \right) \right] \right\} \quad (2)$$

$$a_y = \frac{1}{w} \Im^{-1}\left\{ \frac{1}{\gamma D} \left[-\alpha\beta \left(C_x \Im\{ws_x\} + B_y \Im\{ws_y\} \right) - \left(1-\beta^2\right) \left(C_y \Im\{ws_x\} - B_x \Im\{ws_y\} \right) \right] \right\} \quad (3)$$

respectively. Here, a denotes the probe corrected fields of the AUT, B and C represent the angular spectra of the measuring probes and s are the measured fields, D represents the quantity,

$$D = B_x(-\alpha,\beta) C_x(-\beta,-\alpha) + B_y(-\alpha,\beta) C_y(-\beta,-\alpha) \quad (4)$$

Again, the windowing function w has the same constraints placed upon it as were described above. The crucial importance of this technique is that it enables two or more partial scans to be combined where they have been rotated around more than a single axis as there is no reliance upon convenient co-ordinate systems and polarisation bases.

4.0 Limit of Applicability of the Partial Scan Technique

The success of this windowing technique for the recovery of the normal field component, and thus correspondingly the probe pattern correction, leads to the simple question, what is the limit of how small the partial scan can be made? Specifically, can the partial scans be collapsed to a single one-dimensional strip, or in the limit, a zero-dimensional point?

Clearly, for the windowing technique to be deployable the partial scan must be sufficiently large to enable the application of a smooth amplitude taper. However, as we are only interested in the results at a single point in space, if the near field data were to be extrapolated such that a windowing function could be usefully applied then, although the extrapolated results would be in error, the central point would be handled correctly. The process would consist of the following steps: extrapolate a sufficiently large data set, apply the near field window, reconstruct the normal field component, remove the window, and remove the extrapolated points so that only the normal field component corresponding to the original data points remains. As in the limit only a single field point is known, the only form of extrapolation available is by means of a constant, specifically set the extrapolated data equal to the known field point and allow the windowing function to taper this smoothly to zero. Figure 3 below contains a cut that compares the normal field component having been reconstructed using the entire two-dimensional data set, and the equivalent having been recovered using the extrapolation/windowing method on a single near field cut.

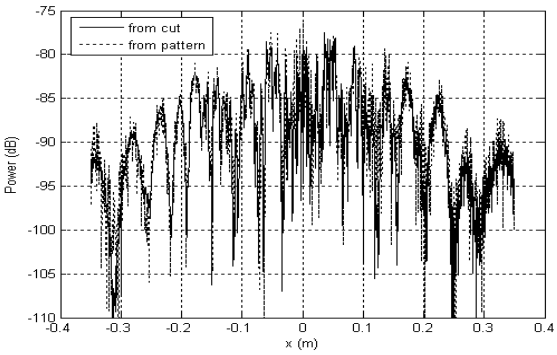

Figure 3 Comparison of reconstructed normal field component recovered from full two-dimensional pattern and single cut

From inspection of Figure 3 above, it can be seen that the degree of agreement is very encouraging with the respective traces being in good agreement over the entire near field region and similarly good results have been attained for the phase pattern. Although further verification is ongoing, this would suggest that this technique could perhaps be used to obtain probe-corrected far field data from measurements taken using any scanning geometry that can be decomposed into a series of one-dimensional linear cuts, for example cylindrical and conical measurement systems.

5.0 Near-field to Far-field Transform of Probe Corrected Data

Generally, modal expansion techniques are inappropriate for use with bespoke (tailored) sampling surfaces, as the sampling surface must correspond to a constant co-ordinate surface in the system for which the harmonic function series solutions are available. Consequently, an alternative technique that better handles discontinuities in the sampling surface than the plane wave spectrum method was sought. To this end, the Kirchhoff-Huygens (KH) formula was utilised [7]. This method essentially constitutes a direct integration of Maxwell's equations with the use of a vector Green's theorem to yield an integral solution of Maxwell's equations in terms of sources, *c.f.* the Stratton-Chu solution. The choice of the field form of this method was thought to be preferable in this case as although an equivalent surface electric and surface magnetic current form of the KH formula exists and is widely used, the quantities that are sampled within the measurement are proportional to fields, *not* surface currents. It is applicable to arbitrary shaped apertures over which both the electric and magnetic fields are prescribed. The far electric field, at a point P radiated by a *closed* Huygens surface S is [4, 7],

$$\underline{E}_p(\underline{\hat{u}}) = \frac{\pi}{jk_0\lambda^2}\int_S \left[\underline{\hat{u}}\times\left(\underline{\hat{n}}\times\underline{E}\right) + Z_0\,\underline{\hat{u}}\times\left\{\left(\underline{\hat{n}}\times\underline{H}\right)\times\underline{\hat{u}}\right\}\right] e^{jk_0\underline{\hat{u}}\cdot\underline{r}}\,da \quad (5)$$

This expression yields the far-field vector pattern function from an integral of the electric and magnetic fields over the closed surface S and da is an elemental area of S and $\underline{n}$ is the outward pointing surface unit normal. Here, the r^{-1} term and the unimportant phase factor have been suppressed as in accordance with the usual convention. The corresponding far magnetic field can be obtained from the electric field using the knowledge that the electric field, magnetic field and direction of propagation are mutually orthogonal.

6.0 Example Results

A cuboidal measurement geometry was chosen to illustrate this novel measurement and transformation process as this constitutes an extreme case for the poly-planar transform since each of the adjacent partial scans will intersect at 90º. Each of the six partial scans was processed using the novel transformation algorithm described. The *y*-polarised electric near field can be found presented in Figure 4 below. As expected, the fields at the intersection between adjacent partial scans are continuous and although not shown here, similarly encouraging results were obtained for other polarisations and for the magnetic fields [4].

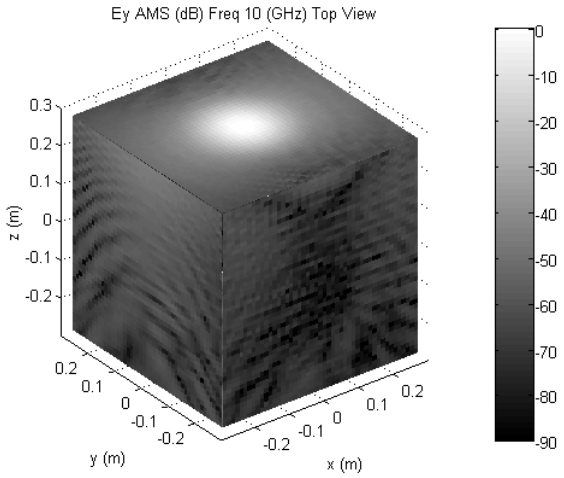

Figure 4 Probe corrected *y*-polarised electric field component.

Here, a mechanically robust, low gain antenna was chosen to be the AUT so that a significant proportion of the radiated field would illuminate the sidewalls of the conceptual sampling cube and susceptibility to gravitational deformation would not be an issue. Thus, the encouraging agreement attained between far-field antenna patterns acquired using a conventional compact antenna test range (CATR) and patterns obtained from the poly-planar technique constituted strong verification that the probe pattern correction, the partial scan

concatenation and the near-field to far-field transformation process had been implemented correctly.

These six probe corrected near field data sets were transformed to the far-field and resolved onto a Ludwig III copular and cross-polar polarisation basis. The copular great circle azimuth cut can be found presented in Figure 5 below.

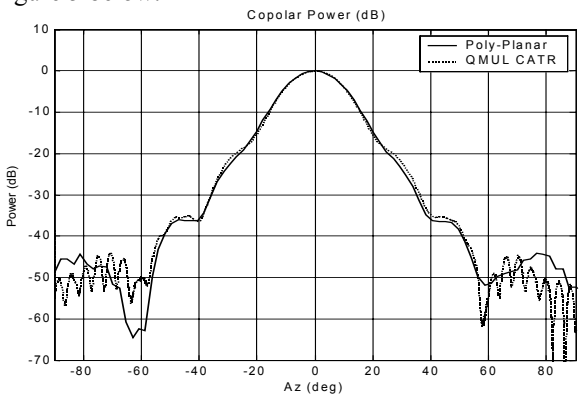

Figure 5 Comparison of azimuth cuts

Here, the black traces represent patterns obtained from the poly-planar technique whilst the dashed traces denote results obtained from the Queen Mary CATR. The high frequency oscillatory behaviour evident within the azimuth cut of the CATR at wide angles is a result of a multiple reflections within the facility and should be ignored. Here, although a good degree of agreement is encouraging some differences are evident. This can be attributed in part to recognising that the six partial scans will not intersect perfectly, and the adverse effects of reflections from scatters within the chamber will degrade the resulting far-field patterns. Corrugated horns are renowned for their symmetry. Consequently, lack of symmetry can often be used as an indication that a measurement is unreliable. Although some asymmetries are apparent, the pattern cut is not excessively asymmetric.

Clearly, as the AUT is located at the centre of a conceptual measurement cube, classically the angle of validity for the front plane would be ±45° in azimuth and elevation. Thus, particular attention should be paid to regions around ±45° as if the transformation were in error, this is where it would be expected to be most noticeable. Crucially, no discernible divergence is observable in this region.

7.0 Conclusions

The measurement process still requires a great deal of refinement. However, for the first time encouraging results, that are free from the high frequency spurious ripples that have plagued all previous attempts, have been obtained. Thus, it would appear that probe corrected spectral techniques could be combined with the KH method to form a hybrid technique that alleviates the deficiencies that render these techniques useless when used individually. It has been shown that with the implementation of suitable extrapolation and windowing techniques, it is possible to collapse the partial scan down to a single cut and still recover the normal field component reliably. Finally, it has been shown that by enclosing a low to medium gain antenna (a corrugated horn) within an imaginary cuboid and measuring the near-field on all six sides of the cuboid, using a suitable rotation of the AUT, a prediction of the full spherical radiation pattern of the antenna can be obtained.

8.0 REFERENCES

[1] S.F. Gregson, J. McCormick, “Image Classification as Applied to the Holographic Analysis of Misaligned Antennas”, 22nd ESTEC Antenna Workshop on Antenna Measurements, 11-12 May 1999, Noordwijk, The Netherlands

[2] A.C. Newell, G. Hindman, “Antenna Spherical Coordinate Systems and their Application in Combining Results from Different Antenna Orientations”, 22nd ESTEC Antenna Workshop on Antenna Measurements, 11-12 May 1999, Noordwijk, The Netherlands

[3] S.F. Gregson, C.G. Parini, J. McCormick, “Wide Angle Antenna Pattern Measurements using a Polyplanar Near-Field Technique”, ICAP, University of Exeter, 2003.

[4] S.F. Gregson, “Probe-Corrected Poly Planar Near-field Antenna Measurements”, Ph.D. Thesis, University of London 2003.

[5] S.F. Gregson, C.G. Parini, J. McCormick, “Development of Wide-Angle Antenna Pattern Measurements using a Probe-Corrected Polyplanar Near-field Measurement Technique”, IEE Proc.-Microw. Antennas Propag., Vol. 152, No. 6, Dec 2005.

[6] R.H. Clarke & J. Brown, “Diffraction Theory and Antennas”, Ellis Horwood Ltd., 1980.

[7] R.S. Elliott, “Antenna Theory and Design, Revised Edition”, Wiley-Interscience, ISBN 0-471-44996-2, 2003.

9.0 ACKNOWLEDGMENTS

The authors wish to acknowledge the financial support from the UK EPSRC in respect to the provision of the near-field measurement facility at Queen Mary, University of London, and to Mr J. Dupuy for taking the measurements.